Model Studies on Calcium-Containing Quinoprotein Alcohol Dehydrogenases. Catalytic Role of Ca^{2+} for the Oxidation of Alcohols by Coenzyme PQQ (4,5-Dihydro-4,5-dioxo-1*H*-pyrrolo[2,3-*f*]quinoline-2,7,9-tricarboxylic Acid)†

Shinobu Itoh,* Hirokatsu Kawakami, and Shunichi Fukuzumi*

Department of Applied Chemistry, Faculty of Engineering, Osaka University, 2-1 Yamada-oka, Suita, Osaka 565-0871, Japan

Received January 5, 1998; Revised Manuscript Received February 20, 1998

ABSTRACT: Mechanistic studies on the action of calcium-containing quinoprotein alcohol dehydrogenases have been performed by using a series of PQQ model compounds in anhydrous organic media. The PQQ model compounds are shown to form 1:1 complexes with a series of alkaline earth metal ions by spectroscopic methods and theoretical calculations. The site of coordination of the PQQ molecule to the metal ions in solution is indicated to be the same as in the case of enzymatic systems. It has also been found that Ca^{2+} binds to the quinone most strongly among the alkaline earth metal ions. Formation of the C-5 hemiacetal derivatives with methanol, ethanol, and 2-propanol is also investigated spectrophotometrically to show that the alcohol addition to the quinone is enhanced in the presence of the metal ions. In this case as well, Ca^{2+} shows the highest efficiency for the enhancement of the C-5 hemiacetal formation. Addition of a strong base such as DBU into an MeCN solution containing the Ca^{2+} complex of the PQQ model compounds and the alcohols leads to the redox reactions to afford reduced PQQ derivatives and the corresponding aldehydes. On the basis of detailed kinetic studies on the redox reactions, including structural effects of PQQ analogues and metal ion effects, we propose the addition−oxidative elimination mechanism through the C-5 hemiacetal intermediate.

Quinoprotein alcohol dehydrogenases (EC 1.1.99.8) comprise a new class of enzymes that involve a heterocyclic *o*-quinone coenzyme PQQ[1] (pyrroloquinolinequinone) as a

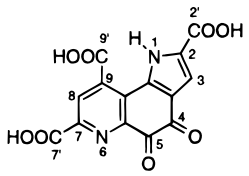

PQQ

redox catalyst for the enzymatic alcohol-oxidation reactions (eq 1) (*1*). Among them, bacterial methanol dehydrogenase

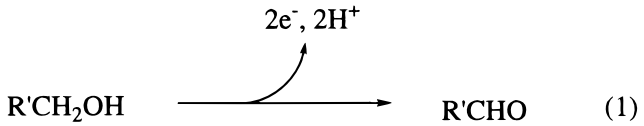

(1)

(MDH) is the most well-characterized and attractive enzyme that catalyzes the oxidation of methanol to formaldehyde, a key step of the biological C_1 metabolism (*2*). One of the most curious feature of this enzyme may be the high reactivity toward lower alkyl alcohols such as methanol despite the relatively low redox potential of free PQQ (*3*).[2] In other words, how does the enzyme activate PQQ to undergo such an energetically difficult oxidation reaction? An addition−elimination through a hemiacetal-type intermediate or an acid−base-catalyzed hydride transfer has so far been discussed as the possible reaction mechanism for the enzymatic alcohol oxidation by PQQ (*4*−*8*). However, more systematic studies are required for a better understanding of the actual mechanism.

Recently, the crystal structure of MDH from methylotrophic bacteria has been determined by two independent research groups, providing full details of the enzyme active center. According to the reported X-ray structure, there is one calcium ion strongly bound to PQQ through its C-5 quinone carbonyl oxygen, N-6 pyridine nitrogen, and C-7 carboxylate group in the enzyme active site (*9*, *10*). Existence of Ca^{2+} in the enzyme active site has also been suggested for other PQQ-dependent enzymes such as ethanol dehydrogenase from *Pseudomonas aeruginosa* and glucose dehydrogenase from *Acinetobacter calcoaceticus* (*11*, *12*).[3]

† This study was financially supported in part by Grants-in-Aid for Scientific Research on a Priority Area (Molecular Biometallics, Grants 08249223 and 09235218) and a Grant-in-Aid for General Scientific Research (Grant 08458177) from the Ministry of Education, Science, Sports, and Culture of Japan. We also thank the Takeda Science Foundation for the financial support.

[1] Abbreviations: PQQ, 4,5-dihydro-4,5-dioxo-1*H*-pyrrolo[2,3-*f*]-quinoline-2,7,9-tricarboxylic acid; DBU, 1,8-diazabicyclo[5.4.0]undec-7-ene.

[2] Methanol can be used as a solvent for several oxidation reactions by highly oxidation-active quinones such as DDQ (2,3-dichloro-5,6-dicyano-1,4-benzoquinone) and *p*-chloranil (tetrachloro-*p*-benzoquinone). The two-electron redox potential of free PQQ (−0.175 V vs SCE at pH 7.0) is much lower than that of DDQ and *p*-chloranil.

[3] I. Willner, E. Katz, and their co-workers prepared PQQ-modified electrodes for the development of bioelectrochemical detectors, where they use Ca^{2+} to control the redox activity of PQQ attached on the electrode surface.

S0006-2960(98)00009-9 CCC: $15.00
Published on Web 04/15/1998

Although Davidson and co-workers have recently suggested that Ca^{2+} plays an important role in the structural stabilization of the enzyme (*13*), little has been known about the catalytic role of Ca^{2+} for the redox reaction in MDH. In this context, we have recently succeeded in demonstrating the methanol oxidation by the calcium complex of PQQ and proposed the addition−oxidative elimination mechanism through the C-5 hemiacetal intermediate (*14*). Here, we report the full details about the catalytic role of alkaline earth metal ions in the oxidation of alcohols by coenzyme PQQ and its analogues to shed light on the redox mechanism of the calcium-containing quinoprotein alcohol dehydrogenases.

MATERIALS AND METHODS

The trimethyl ester of coenzyme PQQ (**2**) was synthesized by esterification of PQQ in methanol by the reported procedures (*15*), and other model compounds, **1** and **3**−**5**, were obtained from the previous studies (*8*, *16*−*18*). All other chemicals used in this study were commercial products of the highest available purity and were further purified by the standard methods, if necessary (*19*). All the alkaline earth metal ions used in this study were obtained as ClO_4^- salts. UV−vis spectra were recorded on a Hewlett-Packard 8452A or a Hewlett-Packard 8453 photodiode array spectrophotometer. ^{1}H NMR and ^{13}C NMR spectra were obtained on a JEOL FT-NMR EX-270 spectrometer. Assignment of the ^{1}H and ^{13}C NMR signals for the three methyl ester groups of **2** has been carried out on the basis of the reported spectral data (*17*). Molecular orbital calculations were performed with the PM3 method by using a Spartan program (Version 4.1, Wavefunction, Inc.). Final geometries and energetics were obtained by optimizing the total molecular energies with respect to all structural variables.

Titration. The binding constants (K_{ML}) for the 1:1 complex formation between the quinones (2.5×10^{-5} M) and alkaline earth metal ions (M^{2+}) were determined by spectrophotometric titration using a 1 cm path length UV cell in anhydrous MeCN at 298 K using eq 2. The data are summarized in Table 2.

The equilibrium constants (K_{add}) for the alcohol addition to the quinones (2.5×10^{-5} M) were determined in the presence and absence of M^{2+} by spectrophotometric titration using a 1 cm path length UV cell in anhydrous MeCN at 298 K. The metal ion concentrations used in the titrations were large enough to convert all the quinone to the corresponding metal complexes (indicated in the figure captions). The analytical procedure has already been reported in the literature (*8*), and the data are summarized in Table 3.

Kinetic Analysis. The redox reactions of the metal complexes of the quinones with the alcohols (ROH) were followed by the UV−vis spectra under pseudo-first-order conditions with excess alcohol in deaerated MeCN at 298 K. Typically, an anhydrous MeCN solution containing the quinone (2.5×10^{-5} M), $M(ClO_4)_2$, and ROH was placed in a UV cell (1 cm path length, sealed tightly with a silicon rubber cap) and was deaerated by bubbling Ar through it for ca. 20 min. Then deaerated DBU was added with a microsyringe to start the reaction. The pseudo-first-order rate constant [$k_{obs(2)}$] was calculated from the rate of a decrease in intensity of the absorption due to the quinone or an increase in intensity of the absorption due to the product. The Mac curve fit (version 1.0) program was used for the nonlinear curve fitting of the plots of $k_{obs(2)}$ versus [ROH] and of $k_{obs(2)}$ versus [DBU] (Figure 8) to obtain the kinetic parameters listed in Tables 4 and 5 (K_a, K_{add}, and k).

Product Analysis. The oxidation products, formaldehyde, acetaldehyde, and acetone, were isolated as the 2,4-dinitrophenylhydrazone derivatives, and their yields were determined by ^{1}H NMR. Typically, an anhydrous MeCN solution (100 mL) containing **2** (5.1 mg, 14 μmol), $Ca(ClO_4)_2$ (203 mg, 0.65 mmol), and EtOH (10 mL, 0.17 mol) was deaerated by bubbling Ar through it for ca. 20 min. Then deaerated DBU (40 mL, 0.27 mmol) was added with a microsyringe to start the reaction, and the mixture was stirred for 8 h at room temperature. Then, 2,4-dinitrophenylhydrazine (50 mg, 0.25 mmol) was added into the solution, and the mixture was stirred for an additional 10 min. Removal of the solvent under reduced pressure gave an orange residue which was dissolved in $CDCl_3$ for the ^{1}H NMR analysis. Formation of 2,4-dinitrophenylhydrazone of acetaldehyde was confirmed by comparing the peaks of the product to those of an authentic sample, and its yield was determined by using tetrachloroethane as an internal reference.

Catalytic oxidation of ethanol by $[Ca(\mathbf{2})]^{2+}$ was carried out in a similar way but under an O_2 atmosphere, and the product analysis was performed with the same procedure as described above.

RESULTS AND DISCUSSION

Metal Ion Binding. Coenzyme PQQ has attracted much attention as a potential metal ligand due to its characteristic structure of the quinolinequinone moiety having a carboxyl group at the α-position of the quinoline nucleus. So far, binding of Na^+, K^+, Cd^{2+}, Cu^{2+}, and Fe^{3+} to PQQ or its analogues has been examined to demonstrate that the molecular cleft surrounded by the quinone carbonyl group at C-5 (O-5), the pyridine nitrogen (N-6), and the carboxylate group at the 7-position (O-7′) is the most suitable place for the metal ion coordination (*20*). Thus, to check the generality of the metal ion binding site of PQQ and to construct an active site model for Ca^{2+}-containing quinoproteins, we first examined the interaction of PQQ and alkaline earth metal ions (M^{2+}) in solution. To avoid complexity coming from the strong interaction between M^{2+} and the water molecule, we performed the model studies using organic solvent soluble PQQ and its analogues (Chart 1) in anhydrous organic media.

When the trimethyl ester of PQQ (**2**) was treated with $Ca(ClO_4)_2$ in anhydrous MeCN, the absorption band at 354 nm due to the quinone shifted to 368 nm and the shoulder around 280 nm decreases with clear isosbestic points at 268, 289, 303, 361, and 422 nm (Figure 1). The binding constant K_{ML} for 1:1 complex formation between the quinone (Q) and the metal ion (M^{2+}) can be expressed by eq 2

$$\frac{A - A_0}{A_\infty - A} = K_{ML}\left([M^{2+}]_0 - \frac{A - A_0}{A_\infty - A}[Q]_0\right) \qquad (2)$$

where A_0 and A_∞ are the initial and final absorptions of the titration and $[M^{2+}]_0$ and $[Q]_0$ denote the concentration of the added metal ion and the initial quinone concentration, respectively. Thus, the plot of $(A - A_0)/(A_\infty - A)$ versus

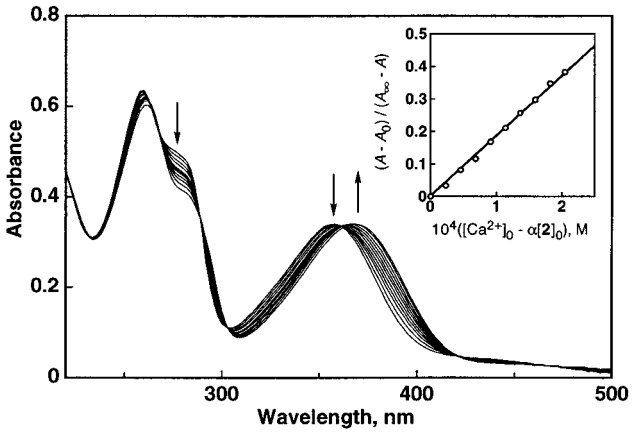

FIGURE 1: Spectral change observed upon addition of $Ca(ClO_4)_2$ ($0-6.5 \times 10^{-3}$ M) to a MeCN solution of **2** (2.5×10^{-5} M) at 298 K. (Inset) Plot of $(A - A_0)/(A_\infty - A)$ vs $[Ca(ClO_4)_2]_0 - \alpha[\mathbf{2}]_0$ [$\alpha = (A - A_0)/(A_\infty - A_0)$] for Ca^{2+} complex formation of **2**.

Chart 1

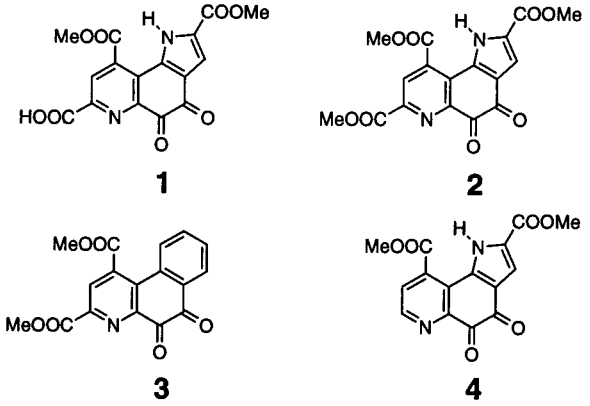

$([Ca^{2+}]_0 - \alpha[\mathbf{2}]_0)$ [$\alpha = (A - A_0)/(A_\infty - A_0)$] gave a straight line passing through the origin as shown in the inset of Figure 1, from which a K_{ML} value of 1900 M^{-1} was obtained as the slope.

Despite our great efforts, a single crystal of the Ca^{2+} complex suitable for the X-ray analysis could not be obtained. However, the ^1H and ^{13}C NMR data in MeCN-d_3 clearly indicate that the position of binding of Ca^{2+} to **2** in acetonitrile is the same as that to PQQ itself in the enzymatic system (type A in Figure 2) as follows. In the ^1H NMR spectra, the methyl ester protons at the 7-position move downfield more than those at the 2- and 9-positions after complexation with Ca^{2+} ($\Delta\delta$ = 0.14, 0.02, and 0.06, respectively) and the $\Delta\delta$ (downfield shift by the complexation) value of H-8 is also larger than that of H-3 (0.09 and 0.07, respectively). In the ^{13}C NMR spectra, C-5 and C-7′ (ester carbonyl carbon at the 7-position) shifted downfield (Δppm = 2.0 and 2.8, respectively), while C-4, C-2′ (ester carbonyl carbon at the 2-position), and C-9′ (ester carbonyl carbon at the 9-position) shifted upfield after complexation with Ca^{2+} (Δppm = −1.0, −0.2, and −1.0, respectively).

Molecular orbital calculations using the Spartan program (version 4.1) also suggest that type A shown in Figure 2 is much more preferable than type B for Ca^{2+} binding.[4] The

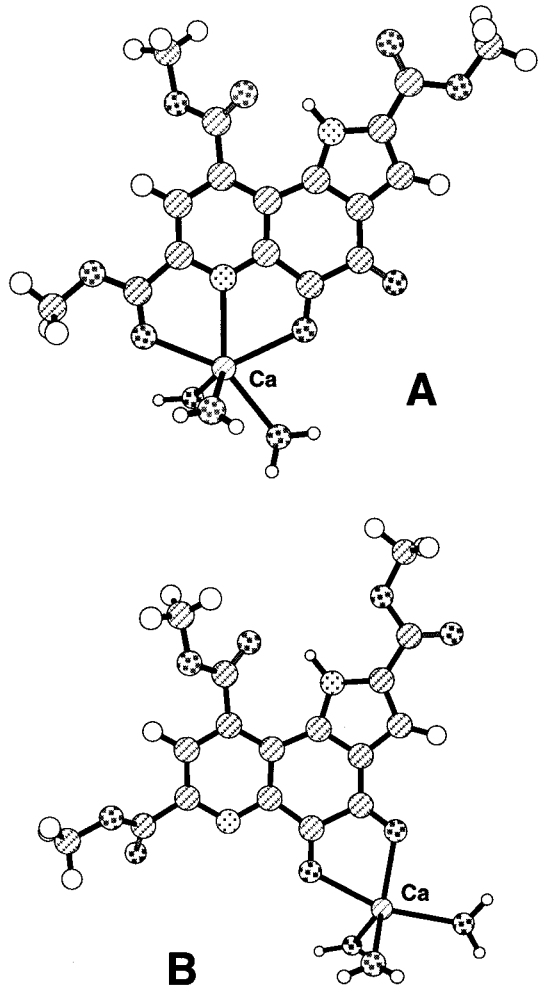

FIGURE 2: Chem3D representations of the optimized structures of $[Ca(\mathbf{2})(H_2O)_3]^{2+}$ by Spartan (version 4.1).

heat of formation ΔH_f of type A is significantly smaller than that of type B (Table 1). Furthermore, the coordination geometry between Ca^{2+} and the PQQ molecule in the enzyme active site (Ca^{2+}−O-5 of 2.50 Å, Ca^{2+}−N-6 of 2.47 Å, and Ca^{2+}−O-7′ of 2.30 Å) (*9b*) is well reproduced in the calculated structure of type A in Figure 2 (Ca^{2+}−O-5′ of 2.43 Å, Ca^{2+}−N-6 of 2.46 Å, and Ca^{2+}−O-7′ of 2.36 Å).

Essentially the same spectral changes (bathochromic shift of the absorption around 355 nm and decrease of the shoulder around 280 nm) were obtained in the titrations of **1** by Ca^{2+} and of **2** by Sr^{2+} and Ba^{2+} (Table 2), implying that the position of binding of the metal ions (Ca^{2+}, Sr^{2+}, and Ba^{2+}) to **1** and **2** is essentially the same (type A in Figure 2). In the titration of **3** and **4** with Ca^{2+}, **3** also shows a similar type of spectral change [bathochromic shift of the absorption at 304 nm and decrease of the shoulder around 270 nm (not shown)], while **4** exhibited a very small shift of the absorption at 342 nm (Table 2). The K_{ML} values of other model compounds (**1**, **3**, and **4**) for binding to Ca^{2+} and for binding of **2** to Sr^{2+} and Ba^{2+} were then determined by analyzing the spectral changes in a similar manner described above, and they are listed in Table 2 together with the λ_{max} of the quinones and their M^{2+} complexes.

As can be expected, the carboxyl group at the 7-position in **1** enhances the binding constant of Ca^{2+}, and its removal in **4** greatly depresses the stability of the Ca^{2+} complex.

[4] Since the calcium ion in the enzyme active site is hexacoordinate (*9*, *10*), we carried out the calculation on the Ca^{2+} complexes of **2** with three water molecules as the external ligands.

Table 1: Heats of Formation of Ca^{2+} and Mg^{2+} Complexes of the Quinones Calculated by Spartan (version 4.1)

complex	ΔH_f (kcal mol^{-1}) type A	type B
$[Ca(\mathbf{1})(H_2O)_3]^{2+}$	−283.3	−245.0
$[Ca(\mathbf{2})(H_2O)_3]^{2+}$	−280.0	−243.2
$[Ca(\mathbf{3})(H_2O)_3]^{2+}$	−192.0	−151.2
$[Ca(\mathbf{4})(H_2O)_3]^{2+}$	−164.3	−165.5
$[Mg(\mathbf{2})(H_2O)_3]^{2+}$	−116.6	−122.5

Table 2: Metal Ion Binding Constants (K_{ML}) and UV−Vis Absorption Maxima (λ_{max}) in MeCN

quinone	M^{2+}	ionic radius[a] (Å)	λ_{max} (nm) quinone	$[M(\mathbf{Q})]^{2+}$	K_{ML} (M^{-1})[b]
1	Ca^{2+}	0.99	356	364	5700
2	Ca^{2+}	0.99	354	368	1900
3	Ca^{2+}	0.99	304	310	750
4	Ca^{2+}	0.99	342	344	90
2	Mg^{2+}	0.66	354	—[c]	<5
2	Sr^{2+}	1.12	354	366	590
2	Ba^{2+}	1.34	354	365	380

[a] Taken from ref *34*. [b] The experimental error is within ±5%. [c] The λ_{max} value could not be determined accurately because of the following hydration reaction of the quinone moiety.

Comparison of the calculated heats of formation between type A and type B of $[Ca(\mathbf{4})(H_2O)_3]^{2+}$ (Table 1) and the different spectral change observed in the titration of **4** with Ca^{2+} mentioned above suggest that the binding mode of Ca^{2+} is type B in the case of quinone **4**, demonstrating the importance of the tridentate binding pocket of the PQQ molecule (O-5, N-6, and O-7′) for strong Ca^{2+} binding. The relatively large K_{ML} value of **2**, compared to that of **3**, is consistent with the fact that the π-electron donor ability of the pyrrole nucleus is larger than that of a simple benzene ring, enhancing the Ca^{2+} binding ability of the conjugated quinone moiety in **2** compared to that in **3**.

On the other hand, binding of Mg^{2+} to **2** is very weak, and addition of excess amount of Mg^{2+} gave us a different spectral change which corresponds to hydration of the *o*-quinone moiety (*21*).[5] Thus, the K_{ML} value for the binding of Mg^{2+} to the quinone was roughly estimated by the spectral change at the very beginning of the titration. Interestingly, the molecular orbital calculations suggest that the binding mode of Mg^{2+} to the *o*-quinone is type B even in the case of quinone **2** (see Table 1). The difference of the position of binding to **2** between Ca^{2+} and Mg^{2+} can be attributed to the difference in the ionic radii of those ions (see Table 2). In fact, the distances of Mg^{2+} to O-5, N-6, and O-7′ in the calculated complex of type A are all around 2.43 Å which is significantly longer than the normal Mg^{2+}−O=C (ca. 2.1 Å) and Mg^{2+}−N_{py} (ca. 2.2 Å) distances (*22*, *23*).

It should be also noted that the binding of Ca^{2+} to the quinone is much stronger than that of Sr^{2+} and Ba^{2+}. This is probably due to the fitting of the metal ions to the molecular cleft of PQQ (type A in Figure 2). In other words, the size of Ca^{2+} fits best to that of the binding pocket of PQQ. In fact, the calculated distances (Ca^{2+}−O-5′ of 2.43 Å, Ca^{2+}−N-6 of 2.46 Å, and Ca^{2+}−O-7′ of 2.36 Å) of the Ca^{2+} model complex in type A are all within the range of the reported values for Ca^{2+}−O=C and Ca^{2+}−N_{py} distances in crystals (ca. 2.4 Å) (*24*, *25*). Coordination of the larger metal ions, Sr^{2+} and Ba^{2+}, to **2** may cause a distortion of the PQQ molecule, making the binding constant K_{ML} of these metal ions smaller than that of Ca^{2+}. Furthermore, addition of an excess amount of a harder Lewis acid such as Mg^{2+} to **2** resulted in the hydration of the *o*-quinone moiety,[5] causing a deactivation of PQQ for the redox reactions as mentioned above. These facts may be some of the reasons why quinoprotein alcohol dehydrogenases selected Ca^{2+} as a cocatalyst from the alkaline earth metal ions.

[5] Addition of a large excess of $Mg(ClO_4)_2$ causes the quinone hydration by the hydrated water in $Mg(ClO_4)_2$ even though the experiment is carried out in anhydrous MeCN.

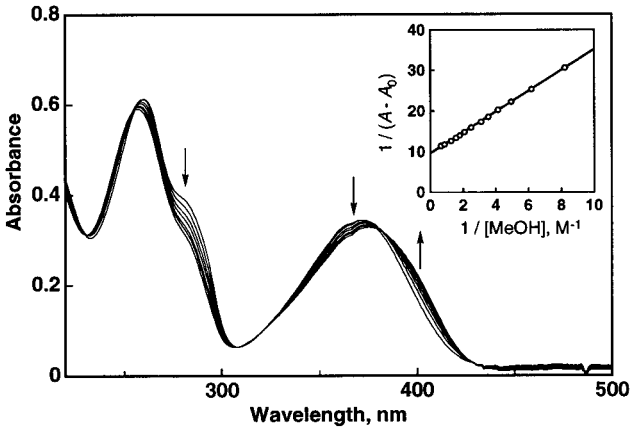

FIGURE 3: Spectral change after the reaction of **2** (2.5×10^{-5} M) with MeOH (0−1.1 M) in the presence of $Ca(ClO_4)_2$ (1.5×10^{-2} M) in MeCN at 298 K. (Inset) Plot of $1/(A - A_0)$ vs 1/[MeOH] for the titration of **2** in the presence of $Ca(ClO_4)_2$ with MeOH.

Hemiacetal Formation. The trimethyl ester of PQQ (**2**) has been shown to provide the corresponding C-5 hemiacetal derivative ($\mathbf{2}_{OMe}$) when it is treated with methanol in MeCN (*8*). The structure of the C-5 hemiacetal derivative $\mathbf{2}_{OMe}$ has been determined by X-ray crystallographic analysis (*8*). Since this reaction is the initial step of the methanol oxidation if it proceeds via the addition−elimination mechanism (*4*), the effects of the alkaline earth metal ions on the hemiacetal formation also merit detailed investigation.

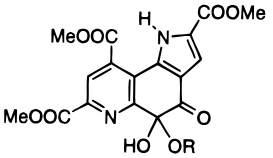

$\mathbf{2}_{OR}$

Addition of methanol to an MeCN solution of $[Ca(\mathbf{2})]^{2+}$ resulted in a spectral change shown in Figure 3 which is characteristic for the C-5 adduct formation (*8*). The equilibrium constant K_{add} for the hemiacetal formation of $[Ca(\mathbf{2})]^{2+}$ with methanol was determined to be 3.6 M^{-1} by the same method reported previously (inset of Figure 3). The K_{add} value thus determined is 6 times larger than that measured in the absence of Ca^{2+} (0.63 M^{-1}) (*8*).

The kinetics for formation of the hemiacetal $\mathbf{2}_{OMe}$ (eq 3) was also examined in the presence and absence of Ca^{2+} by monitoring the time course of the absorbance (A_t) at 354 nm due to the quinone at various methanol concentrations

Table 3: Hemiacetal Formation Constant of Quinone **2** in the Presence and Absence of M^{2+} in MeCN

	K_{add} $(M^{-1})^a$			
alcohol	without M^{2+}	with Ca^{2+}	with Sr^{2+}	with Ba^{2+}
methanol	0.63	3.6	1.1	1.0
ethanol	0.20	1.2	0.74	0.41
2-propanol	0.019	0.32	0.27	0.16

[a] The experimental error is within ±5%.

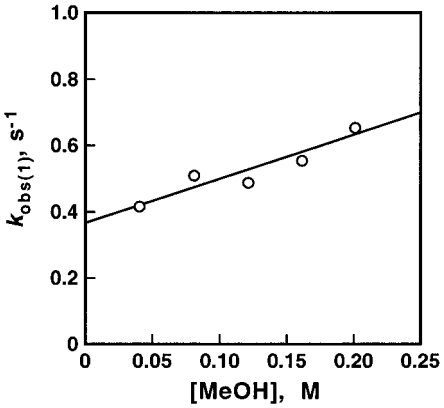

FIGURE 4: Plot of $k_{obs(1)}$ vs [MeOH] for the addition reaction of MeOH with **2** (2.5×10^{-5} M) in the presence of $Ca(ClO_4)_2$ (1.5×10^{-5} M) in MeCN at 298 K.

[ROH] (R = Me).

$$[Ca(\mathbf{2})]^{2+} + ROH \underset{k_b}{\overset{k_f}{\rightleftharpoons}} [Ca(\mathbf{2}_{OR})]^{2+} \quad (3)$$

The decrease in A_t obeys pseudo-first-order kinetics; plots of $\log(A_t - A_{obs})$ against time (t) gave a straight line at each ROH concentration. From the slope of the linear plot is determined the pseudo-first-order constant $k_{obs(1)}$ by using eq 4

$$\ln[(A_0 - A_f)/(A_t - A_f)] = k_{obs(1)}t \quad (4)$$

where A_0 and A_f are the initial and final absorbance in the reaction, respectively. According to eq 3, the pseudo-first-order rate constant $k_{obs(1)}$ is given as a function of [ROH] by eq 5.

$$k_{obs(1)} = k_f[ROH] + k_b \quad (5)$$

The k_f and k_b values were determined to be 1.3 M^{-1} s^{-1} and 0.37 s^{-1}, respectively, from the slope and intercept of the plot of $k_{obs(1)}$ versus [ROH] as indicated in Figure 4. From these rate constants, the equilibrium constant for the hemiacetal formation is calculated to be 3.5 M^{-1} by using the relation $K_{add} = k_f/k_b$, which agrees well with the K_{add} value determined independently by the titration (K_{add} = 3.6 M^{-1}, Figure 3). In the absence of Ca^{2+}, the k_f and k_b values were also determined in a similar manner to be 0.53×10^{-3} M^{-1} s^{-1} and 1.0×10^{-3} s^{-1}, respectively. The K_{add} value determined to be 0.53 M^{-1} from these rate constants is also consistent with the value determined by the titration (0.63 M^{-1}). Judging from these k_f and k_b values, Ca^{2+} complex formation accelerates the methanol addition (k_f) by ca. 2500-fold, while acceleration of the back reaction (k_b) is only ca. 370-fold. The difference in the acceleration effects of Ca^{2+} between the forward and back reactions corresponds to the hemiacetal stabilization effect by Ca^{2+}. Essentially the same spectral changes were obtained in the titrations of **2** by other alcohols such as ethanol and 2-propanol in the presence and absence of the metal ions, and the K_{add} value of each system was determined in the same way (Table 3). The K_{add} value is becoming smaller with the increase in the steric hindrance of the alkyl group of the substrates. In all cases, the Ca^{2+} binding stabilizes the hemiacetal derivatives, resulting in K_{add} values at least 6 times larger than that obtained in the absence of the metal ion. It should be also noted that Ca^{2+} stabilizes the hemiacetal derivatives most efficiently among the three metal ions examined. The smaller stabilizing effect of Sr^{2+} and Ba^{2+} compared to that of Ca^{2+} could be attributed to a steric repulsion between the larger metal ions and the alkyl group of the substrate.

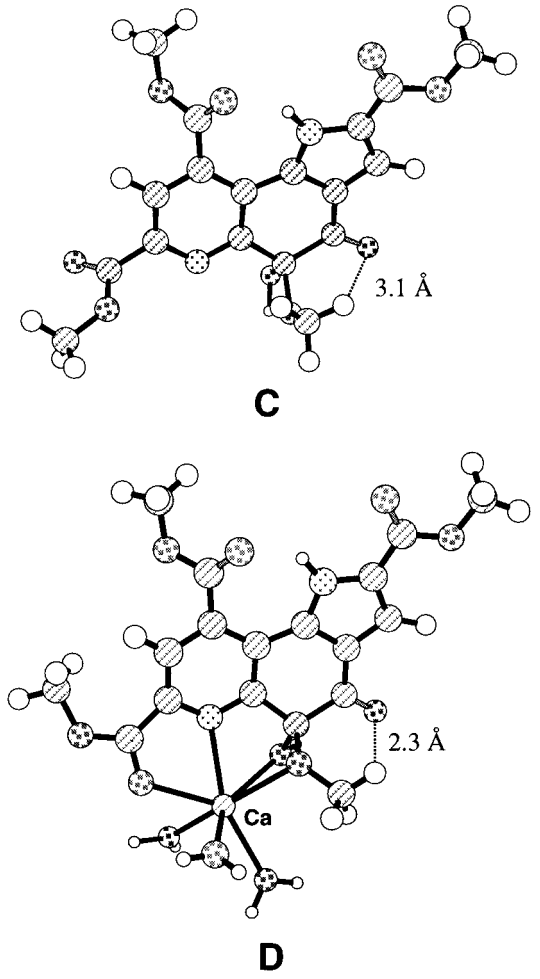

FIGURE 5: Chem3D representations of the optimized structures of $\mathbf{2}_{OMe}$ and $[Ca(\mathbf{2}_{OMe})(H_2O)_3]^{2+}$ by Spartan (version 4.1).

In Figure 5 are shown the computer-generated structures of $\mathbf{2}_{OMe}$ and its Ca^{2+} complex using the Spartan program. The crystal structure of $\mathbf{2}_{OMe}$ (*8*) is well reproduced by the semiempirical molecular orbital calculation with the Spartan program (**C** in Figure 5). In the case of the Ca^{2+} complex of the C-5 hemiacetal (**D** in Figure 5), the metal ion is coordinated by both oxygen atoms of the hemiacetal function (OH and OMe), and this coordination forces the methyl group of the added alcohol moiety (OMe) to flip toward the carbonyl oxygen at the 4-position. Thus, the distance between the carbonyl oxygen at the 4-position and the methyl proton of the added substrate in the Ca^{2+} complex of $\mathbf{2}_{OMe}$

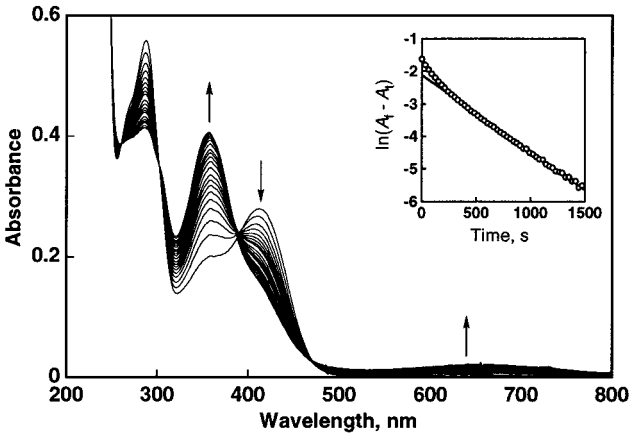

FIGURE 6: Spectral change observed in the oxidation of EtOH (1.1 M) by **2** (2.5×10^{-5} M) in the presence of $Ca(ClO_4)_2$ (6.3×10^{-3} M) and DBU (1.2×10^{-3} M) in deaerated MeCN at 298 K. (Inset) Pseudo-first-order plot based on the absorption change at 358 nm due to the reduced PQQ ($A_f - A_t$, where A_f and A_t are the final absorbance and the absorbance at time t, respectively).

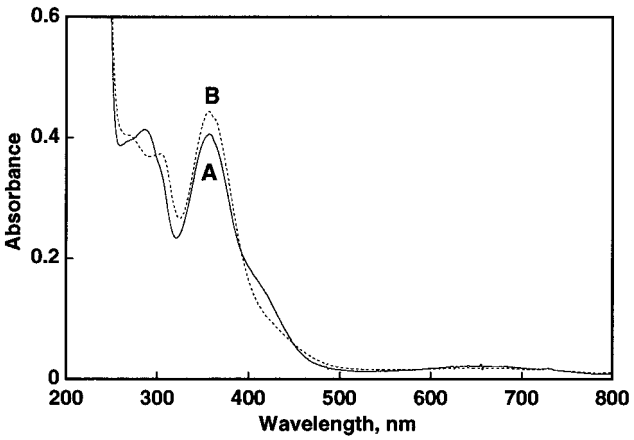

FIGURE 7: Comparison of the UV−visible spectra of (A) the final product of the reaction shown in Figure 6 and (B) the authentic sample of $\mathbf{2H_2}$ under the same experimental conditions.

(**D**) becomes ca. 2.3 Å, which is significantly shorter than that in the hemiacetal itself (3.1 Å, **C**). This seems to indicate that the neighboring carbonyl oxygen at the 4-position could act as a general base to accept the α-proton of the substrate, a possibility discussed below.

Base-Catalyzed Alcohol Oxidation. Addition of the alcohol to a deaerated MeCN solution containing $[Ca(\mathbf{2})]^{2+}$ and a strong base such as DBU resulted in formation of reduced PQQ ($\mathbf{2H_2}$). In Figure 6 is shown a representative example of the spectral change obtained in the reaction with ethanol. The final spectrum of the reaction mixture is essentially the same as that obtained by the treatment of authentic $\mathbf{2H_2}$ (quinol form) (*26*) with $Ca(ClO_4)_2$ and DBU in deaerated MeCN (Figure 7), and it is also very close to the absorption spectrum of fully reduced MDH (*27*).[6] From the reaction mixture in a preparative scale [[**2**] = 1.4×10^{-4} M, $[Ca(ClO_4)_2] = 5.9 \times 10^{-3}$ M, [DBU] = 2.4×10^{-3} M, and [EtOH] = 1.5 M in 100 mL of MeCN], acetaldehyde was isolated quantitatively as the 2,4-dinitrophenylhydrazone derivative. Essentially the same spectral changes were obtained in the reactions with methanol and 2-propanol, and the oxidation products, formaldehyde and acetone, were also obtained as the 2,4-dinitrophenylhydrazone derivatives in 20 and 95% yields, respectively. The low yield of formaldehyde is attributed to its instability under the experimental conditions, since the authentic sample of formaldehyde decomposes under the same experimental conditions.

A first-order plot for the rate of formation of the reduced PQQ is shown in the inset of Figure 6, where there is a quick change at the very beginning of the reaction. This is probably due to the time required for establishment of the pre-equilibrium shown in Scheme 1. Indeed, it has been well demonstrated that the hemiacetal derivative easily reverts to the original quinone when an amine base is added to its solution (*8*) and that deprotonation of the pyrrole proton (1-NH) of **2** results in an increase of absorption at 360 nm (*28*) which is almost identical to the absorption of the reduced PQQ in this system (358 nm). The formation of the reduced PQQ obeys a clean pseudo-first-order kinetics at later reaction time. The pseudo-first-order rate constant [$k_{obs(2)}$] thus obtained shows a Michaelis−Menten type saturation dependence with respect to the ethanol concentration as indicated in Figure 8A. Nonlinear curve fitting using eq 6, derived from the addition−elimination mechanism shown in Scheme 1, provided the following kinetic parameters: $K_a = 1.0 \times 10^3$ M^{-1}, $K_{add} = 1.1$ M^{-1}, and $k = 2.1$ M^{-1} s^{-1}

$$k_{obs(2)} = kK_{add}[ROH][DBU]/(1 + K_a[DBU] + K_{add}[ROH]) \quad (6)$$

where K_a is the deprotonation equilibrium constant ($\mathbf{2}^-$ represents the deprotonated derivative at N-1 of **2**) and k is the rate constant of the oxidative elimination of the product from $[Ca(\mathbf{2}_{OR})]^{2+}$ for producing $[Ca(\mathbf{2H_2})]^{2+}$ and R′CHO (the possibility of the base-catalyzed hydride transfer mechanism is discussed below). The dependence of $k_{obs(2)}$ versus [DBU] (Figure 8B) also afforded a similar saturation phenomenon as expected from the kinetic equation (eq 6), from which the following values were derived with the computer simulation: $K_a = 1.1 \times 10^3$ M^{-1}, $K_{add} = 1.2$ M^{-1}, and $k = 2.2$ $M^{-1}s^{-1}$. The agreements of those kinetic parameters determined independently from $k_{obs(2)}$ versus [ROH] and $k_{obs(2)}$ versus [DBU] as well as K_{add} determined by the titration (1.2 M^{-1}) and kinetics (1.1 and 1.2 M^{-1}) support the validity of the proposed addition−elimination mechanism (*14*). A large kinetic isotope effect ($k_H/k_D = 6.1$) on the rate constant k was obtained by using ethanol-d_6 as a substrate, clearly indicating that the base-catalyzed α-proton abstraction from the substrate is rate-determining in the ethanol oxidation reaction (in the case of methanol; $k_H/k_D = 6.4$).

The kinetic parameters (K_{add}, k, and K_a) for the oxidation of methanol and 2-propanol by $[Ca(\mathbf{2})]^{2+}$ and for the oxidation of ethanol by $[Sr(\mathbf{2})]^{2+}$ and by $[Ba(\mathbf{2})]^{2+}$ were obtained with the same procedures, and they are summarized in Table 4. In all cases, the K_{add} values determined independently from the plots of $k_{obs(2)}$ versus [ROH] and from the plots of $k_{obs(2)}$ versus [DBU] agree well and are essentially the same as those determined by the titrations (Table 2). Thus, the oxidation of these alcohols may proceed via the same addition−elimination mechanism.

[6] The reported UV−vis spectra of the oxidized form of MDH are quite different depending on the conditions, making it difficult for us to compare the spectrum of the Ca^{2+} complex of PQQ to that of the enzyme.

Scheme 1

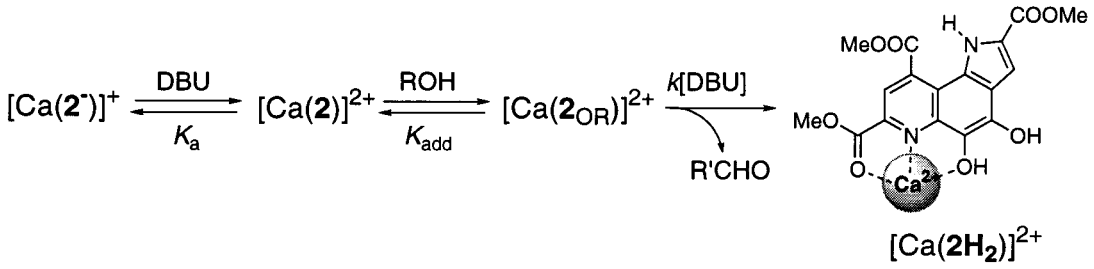

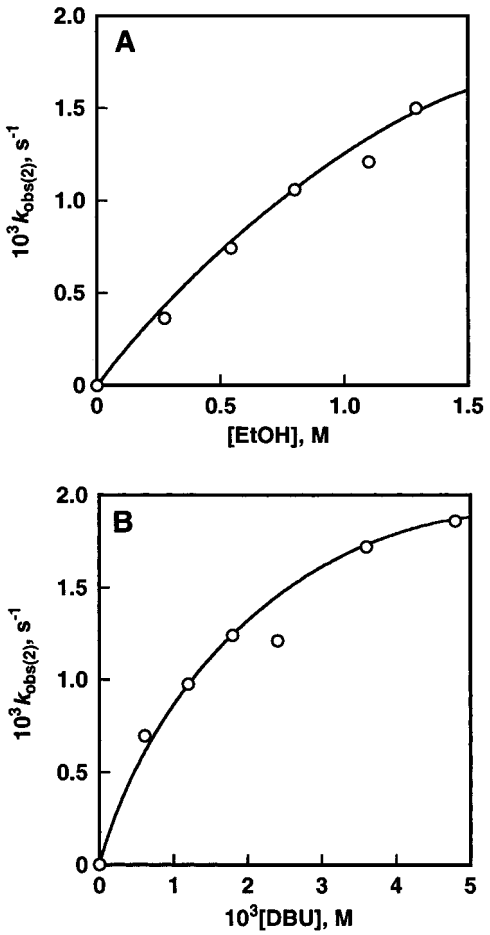

FIGURE 8: Plots of (A) $k_{obs(2)}$ vs [EtOH] for the oxidation of EtOH by **2** (2.5×10^{-5} M) in the presence of $Ca(ClO_4)_2$ (6.3×10^{-3} M) and DBU (2.4×10^{-3} M) and (B) $k_{obs(2)}$ vs [DBU] for the oxidation of EtOH (1.1 M) by **2** (2.5×10^{-5} M) in the presence of $Ca(ClO_4)_2$ (6.3×10^{-3} M) and DBU in deaerated MeCN at 298 K.

Table 4: Kinetic Parameters for the Oxidation of Alcohols by $[M(2)]^{2+}$ in MeCN[a]

alcohol	M^{2+}	K_{add} (M^{-1})[b]	k (M^{-1} s^{-1})[b]	K_a (M^{-1})[b]
methanol	Ca^{2+}	3.7 (3.5)	0.42 (0.42)	1.4×10^3 (1.5×10^3)
ethanol	Ca^{2+}	1.1 (1.2)	2.1 (2.2)	1.0×10^3 (1.1×10^3)
2-propanol	Ca^{2+}	0.30 (0.30)	1.1 (1.1)	5.0×10^2 (5.9×10^2)
ethanol	Sr^{2+}	0.79 (0.79)	40 (39)	2.6×10^3 (2.4×10^3)
ethanol	Ba^{2+}	0.41 (0.41)	150 (160)	5.0×10^3 (5.3×10^3)

[a] Obtained from the plots of k_{obs} vs [ROH]. The kinetic parameters obtained from the plots of $k_{obs(2)}$ vs [DBU] are also shown in parentheses. [b] The experimental error is within ±5%.

In the enzymatic systems, it is known that secondary alkyl alcohols are hardly oxidized by MDH (*29*). In our model system, however, 2-propanol, which is a secondary alkyl alcohol, was also oxidized efficiently as in the case of primary alkyl alcohols such as methanol and ethanol (ethanol > 2-propanol > methanol in k, Table 4), although the K_{add} value of 2-propanol is much smaller than that of methanol and ethanol due to the steric hindrance of the larger alkyl group of 2-propanol. Judging from these results, it can be concluded that the substrate specificity observed in the enzymatic system can be attributed to the incorporation process of the substrate into the enzyme active pocket. In other words, the substrate specificity in the enzymatic reaction is dictated by the dimensions of the enzyme active site.

Scheme 2

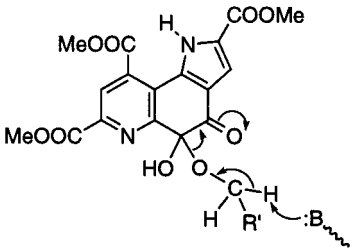

Scheme 3

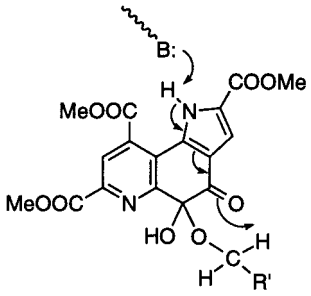

The catalytic efficiency of a series of alkaline and alkaline earth metal ions has been also examined in the oxidation of ethanol. It has been found that the monovalent cations such as Li^+, Na^+, and K^+ and a small divalent cation such as Mg^{2+} are not effective at all while the divalent cations such as Sr^{2+} and Ba^{2+} accelerate the oxidative elimination process (k) much more effectively than Ca^{2+} ($Ba^{2+} > Sr^{2+} > Ca^{2+}$, Table 4). It should be pointed out that the orders of the kinetic parameters (k and K_{add}) of these metal ions are exactly the same as those observed in the enzymatic system (V_{max} and K_m) (*30*). The reason for such a difference in reactivity among these cations is discussed below.

Mechanistic Consideration of the Base-Catalyzed Oxidative Elimination Process. For the oxidative elimination process in the enzymatic system, aspartate (Asp-303) has been suggested to be the most likely candidate for the general base catalyst for the direct α-proton abstraction from the added substrate (Scheme 2) (*9*, *10*). Alternatively, however,

Table 5: Kinetic Parameters for the Oxidation of Ethanol by the Ca^{2+} Complex of **2**, **3**, and **5** in the Presence of DBU in MeCN[a]

quinone	K_{add} (M^{-1})[b]	k (M^{-1} s^{-1})[b]
2	1.1 (1.2)	2.1
3	9.0 (9.0)	0.61
5	3.5 (4.8)	0.55

[a] The K_{add} value determined by the titration of the Ca^{2+} complex of the quinone by ethanol in MeCN is shown in parentheses. [b] The experimental error is within ±5%.

intramolecular general base catalysis by the C-4 carbonyl oxygen induced by deprotonation of the pyrrole proton at N-1 could be expected as has been demonstrated in the amine-oxidation reaction by PQQ (Scheme 3) (*28*). To address this issue, we compared the reactivity of **2** with that of **3** and **5**. Model compounds **3** and **5** do not have such an active pyrrole proton, deprotonation of which will produce a negative charge on the quinone carbonyl oxygen (like a H-1 in **2**). Thus, the kinetic equation (eq 6) can be simplified as eq 7.

$$k_{obs(2)} = kK_{add}[ROH][DBU]/(1 + K_{add}[ROH]) \quad (7)$$

According to eq 7, we can expect a Michaelis−Menten type saturated dependence of $k_{obs(2)}$ with respect to [ROH] as in the case of **2**, but a linear dependence passing through the origin with respect to [DBU]. Those expected relations of $k_{obs(2)}$ versus [ROH] and $k_{obs(2)}$ versus [DBU] have been obtained as shown in Figure 9, confirming the validity of the reaction mechanism illustrated in Scheme 1. From the plots of $k_{obs(2)}$ versus [ROH] (Figure 9A) are determined the kinetic parameters K_{add} and k by the computer curve fitting as summarized in Table 5. In this case as well, the K_{add} values for **3** and **5** with ethanol obtained from the kinetic analysis agree well with those determined independently by the titration (K_{add} values are shown in parentheses in Table 5).

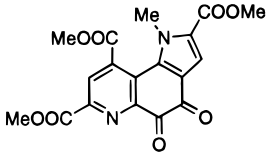

5

We have already demonstrated that the order of reactivity for the C-5 adduct formation with methanol, acetone, and amines is **3** > **5** > **2** (*8*, *16*, *28*, *31*). This tendency of the reactivity is preserved in the C-5 hemiacetal formation with ethanol as shown in Table 5. In general, hydration or alcohol addition to carbonyl compounds is largely enhanced when the carbonyl compounds have a highly electron-withdrawing substituent (*32*). The pyrrole ring, on the other hand, has an opposite effect (an electron-releasing nature), which may be the main reason for the lower reactivity of **2** and **5** as compared to **3**. A small difference in K_{add} between **2** and **5** may reflect the increase in steric hindrance around the 1-position due to replacement of H-1 with the methyl group. Such steric hindrance could be diminished to some extent by adduct formation. In contrast to the hemiacetal formation step (K_{add}), the oxidative elimination process k proceeds most efficiently with the Ca^{2+} complex of **2** among the three

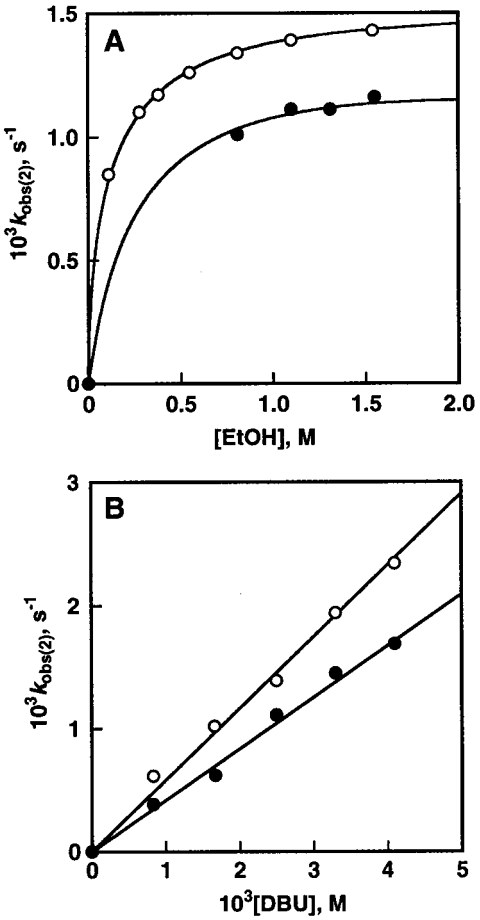

FIGURE 9: Plots of (A) k_{obs} vs [EtOH] for the oxidation of EtOH by (○) **3** (2.6×10^{-5} M) and by (●) **5** (2.5×10^{-5} M) in the presence of $Ca(ClO_4)_2$ ($9.1-9.7 \times 10^{-3}$ M) and DBU (2.5×10^{-3} M) in deaerated MeCN at 298 K and (B) k_{obs} vs [DBU] for the oxidation of EtOH (1.1 M) by (●) **3** (2.6×10^{-5} M) and by (○) **5** (2.5×10^{-5} M) in the presence of $Ca(ClO_4)_2$ ($9.1-9.7 \times 10^{-3}$ M) and DBU in deaerated MeCN at 298 K.

(Table 5). This result may be in part attributed to the contribution of intramolecular general base catalysis by the C-4 quinone carbonyl oxygen as illustrated in Scheme 3. Deprotonation of the pyrrole proton of **2** may increase the negative charge on the C-4 quinone carbonyl oxygen, enhancing the α-proton abstraction of the added substrate. The possibility of such an intramolecular general base catalysis by the C-4 quinone carbonyl oxygen has been also suggested by the theoretical calculations [shorter distance between the α-proton of the substrate and C-4 carbonyl oxygen in $[Ca(\mathbf{2}_{OMe})]^{2+}$ than that in $\mathbf{2}_{OMe}$ itself, see Figure 5].

The order of the catalytic efficiency on the oxidative elimination process (k) is $Ca^{2+} < Sr^{2+} < Ba^{2+}$ (Table 4), which is identical to the order of the ion size ($Ca^{2+} < Sr^{2+} < Ba^{2+}$, see Table 1). This result can be also explained by the intramolecular general base catalysis by C-4 carbonyl oxygen. Namely, the binding of larger metal ions such as Ba^{2+} and Sr^{2+} to the hemiacetal of PQQ forces the added alcohol moiety closer to the C-4 quinone carbonyl oxygen than in the case of Ca^{2+}, letting the α-proton abstraction by the carbonyl oxygen easier.

In summary, we have presented unequivocal evidence of the addition−elimination mechanism through the C-5 hemiacetal intermediate for the oxidation of alcohols by coenzyme

PQQ. In this reaction mechanism, Ca^{2+} plays an important role for acceleration of the alcohol addition, stabilization of the C-5 hemiacetal intermediate thus formed, and enhancement of the α-proton abstraction step by the C-4 carbonyl oxygen (intramolecular catalysis). Furthermore, we have demonstrated that the substrate specificity in the enzymatic reaction may be dictated by the dimensions of the enzyme active site. A base-catalyzed hydride transfer mechanism which involves the calcium complex of the C-5 hemiacetal $[Ca(\mathbf{2}_{OR})]^{2+}$ as a bystander in a side equilibrium is kinetically indistinguishable from the proposed addition−elimination mechanism involving $[Ca(\mathbf{2}_{OR})]^{2+}$ as the real active species. However, the orders of the reactivity in the oxidative elimination process (k) of other model compounds (**2** > **3** > **5**) and of alkaline earth metal ions ($Ca^{2+} < Sr^{2+} < Ba^{2+}$) can only be explained by taking into account the intramolecular general base catalysis by the C4 carbonyl oxygen in the hemiacetal intermediate, strongly supporting the validity of the proposed addition−elimination mechanism.

Finally, we also emphasize that the oxidation of ethanol to acetaldehyde proceeded catalytically (1450% based on **2** after 65 h), when the reaction was carried out under aerobic conditions. In this system, molecular oxygen acts as an electron acceptor to regenerate the quinone from the reduced PQQ. Catalytic effects of Ca^{2+} on the reoxidation process of the reduced PQQ and of NH_3 (activator of quinoprotein alcohol dehydrogenases) on the alcohol-oxidation reaction are now under investigation, and some of the preliminary results were reported elsewhere (*18*, *33*).

REFERENCES

1. Duine, J. A. (1991) *Eur. J. Biochem. 200*, 271.
2. (a) Salisbury, S. A., Forrest, H. S., Cruse, W. B. T., and Kennard, O. (1979) *Nature 280*, 843. (b) Anthony, C. (1993) in *Principles and Applications of Quinoproteins* (Davidson, V. L., Ed.) pp 17−45, Marcel Dekker, Inc., New York. (c) Anthony, C., Ghosh, M., and Blake, C. C. F. (1994) *Biochem. J. 304*, 665.
3. Kano, K., Mori, K., Uno, B., Kubota, T., Ikeda, T., and Senda, M. (1990) *Bioelectrochem. Bioenerg. 23*, 227.
4. Anthony, C. (1996) *Biochem. J. 320*, 697.
5. Frank, J., Jr., van Krimpen, S. H., Verwiel, P. E. J., Jongejan, J. A., Mulder, A. C., and Duine, J. A. (1989) *Eur. J. Biochem. 184*, 187.
6. (a) Andrés, J., Moliner, V., and Krechl, J. (1994) *Bioorg. Chem. 22*, 58. (b) Andrés, J., Moliner, V., Domingo, L. R., Picher, M. T., and Krechl, J. (1995) *J. Am. Chem. Soc. 117*, 8807.
7. Eckert, T. S., Bruice, T. C., Gainor, J. A., and Weinreb, S. M. (1982) *Proc. Natl. Acad. Sci. U.S.A. 79*, 2533.
8. Itoh, S., Ogino, M., Fukui, Y., Murao, H., Komatsu, M., Ohshiro, Y., Inoue, T., Kai, Y., and Kasai, N. (1993) *J. Am. Chem. Soc. 115*, 9960.
9. (a) White, S., Boyd, G., Mathews, F. S., Xia, Z.-x., Dai, W.-w., Zhang, Y.-f., and Davidson, V. L. (1993) *Biochemistry 32*, 12955. (b) Xia, Z.-x., Dai, W.-w., Zhang, Y.-f., White, S. A., Boyd, G. D., and Mathews, F. S. (1996) *J. Mol. Biol. 259*, 480.
10. (a) Blake, C. C. F., Ghosh, M., Harlos, K., Avezoux, A., and Anthony, C. (1994) *Nat. Struct. Biol. 1*, 102. (b) Cozier, G. E., Giles, I. G., and Anthony, C. (1995) *Biochem. J. 308*, 375. (c) Ghosh, M., Anthony, C., Harlos, K., Goodwin, M. G., and Blake, C. (1995) *Structure 3*, 177.
11. (a) Mutzel, A., and Görisch, H. (1991) *Agric. Biol. Chem. 55*, 1721. (b) Geiger, O., and Görisch, H. (1989) *Biochem. J. 261*, 415.
12. (a) Lion-Dagan, M., Katz, E., and Willner, I. (1994) *J. Am. Chem. Soc. 116*, 7913. (b) Katz, E., Lötzbeyer, T., Schlereth, D. D., Schuhmann, W., and Schmidt, H.-L. (1994) *J. Electroanal. Chem. 373*, 189. (c) Katz, E., Lion-Dagan, M., and Willner, I. (1995) *J. Electroanal. Chem. 382*, 25. (d) Bardea, A., Katz, E., Bückmann, A. F., and Willner, I. (1997) *J. Am. Chem. Soc. 119*, 9114.
13. Harris, T. K., and Davidson, V. L. (1994) *Biochem. J. 303*, 141.
14. Itoh, S., Kawakami, H., and Fukuzumi, S. (1997) *J. Am. Chem. Soc. 119*, 439.
15. Itoh, S., Mure, M., Suzuki, A., Murao, H., and Ohshiro, Y. (1992) *J. Chem. Soc., Perkin Trans. 2*, 1245.
16. Itoh, S., Fukui, Y., Haranou, S., Ogino, M., Komatsu, M., and Ohshiro, Y. (1992) *J. Org. Chem. 57*, 4452.
17. Itoh, S., Kato, J., Inoue, T., Kitamura, Y., Komatsu, M., and Ohshiro, Y. (1987) *Synthesis*, 1067.
18. Itoh, S., Huang, X., Kawakami, H., Komatsu, M., Ohshiro, Y., and Fukuzumi, S. (1995) *J. Chem. Soc., Chem. Commun.*, 2077.
19. Perrin, D. D., Armarego, W. L. F., and Perrin, D. R. (1966) *Purification of Laboratory Chemicals*, Pergamon Press, Elmsford, NY.
20. (a) Noar, J. B., Rodriguez, E. J., and Bruice, T. C. (1985) *J. Am. Chem. Soc. 107*, 7198. (b) Suzuki, S., Sakurai, T., Itoh, S., and Ohshiro, Y. (1988) *Inorg. Chem. 27*, 591. (c) Ishida, T., Doi, M., Tomita, K., Hayashi, H., Inoue, M., and Urakami, T. (1989) *J. Am. Chem. Soc. 111*, 6822. (d) Schwederski, B., Kasack, V., Kaim, W., Roth, E., and Jordanov, J. (1990) *Angew. Chem., Int. Ed. Engl. 29*, 78. (e) Nakamura, N., Kohzuma, T., Kuma, H., and Suzuki, S. (1994) *Inorg. Chem. 33*, 1594. (f) Tommasi, T., Shechter-Barloy, L., Varech, D., Battioni, J.-P., Donnadieu, B., Verelst, M., Bousseksou, A., Mansuy, D., and Tuchagues, J.-P. (1995) *Inorg. Chem. 34*, 1514.
21. Dekker, R. H., Duine, J. A., Frank, J., Verwiel, P. E. J., and Westerling, J. (1982) *Eur. J. Biochem. 125*, 69.
22. (a) Hoyer, M., and Hartl, H. (1992) *Z. Anorg. Chem. 612*, 45. (b) Di Noto, V., Bandoli, G., Dolmella, A., Zarli, B., Viviani, M., and Vidali, M. (1995) *J. Chem. Crystallogr. 25*, 375. (c) Bergstrom, R., Satyshur, K., and Sundaralingam, M. (1981) *Acta Crystallogr., Sect. B 37*, 254.
23. (a) Henderson, M. J., Papasergio, R. I., Raston, C. L., White, A. H., and Lappert, M. F. (1986) *J. Chem. Soc., Chem. Commun.*, 672. (b) Englehart, L. M., Junk, P. C., Patalinghug, W. C., Sue, R. E., Raston, C. L., Skelton, B. W., and White, A. H. (1991) *J. Chem. Soc., Chem. Commun.*, 930. (c) Constable, E. C., Healy, J., and Dren, M. G. B. (1991) *Polyhedron 10*, 1883. (d) Henderson, K. W., Mulvey, R. E., Clegg, W., and O'Neil, P. A. (1992) *J. Organomet. Chem. 439*, 237. (e) Lipkowski, J., and Soldatov, D. (1993) *J. Coord. Chem. 28*, 265. (f) Deloume, J.-P., Loiseleur, H., and Thomas, G. (1973) *Acta Crystallogr., Sect. B 29*, 668. (g) Halut-Desportes, S. (1977) *Acta Crystallogr., Sect. B 33*, 599. (h) Waters, A. F., and White, A. H. (1996) *Aust. J. Chem. 49*, 35.
24. (a) Lewinski, K., and Lebioda, L. (1986) *J. Am. Chem. Soc. 108*, 3693. (b) Rao, C. P., Rao, A. M., and Rao, C. N. R. (1984) *Inorg. Chem. 23*, 2080. (c) Seebach, D., Hansen, J., Seiler, P., and Gromek, J. M. (1985) *J. Organomet. Chem. 285*, 1. (d) Gentile, P. S., White, J. G., Dinstein, M. P., and Bray, D. D. (1977) *Inorg. Chim. Acta 21*, 141. (e) Pavanello, L., Visona, P., Marigo, A., Bresadola, S., and Valle, G. (1994) *Inorg. Chim. Acta 216*, 261.
25. Halut-Desportes, S. (1981) *Rev. Chim. Miner. 18*, 199.
26. Itoh, S., Ohshiro, Y., and Agawa, T. (1986) *Bull. Chem. Soc. Jpn. 59*, 1911.

27. (a) Frank, J., Dijkstra, M., Duine, J. A., and Balny, C. (1988) *Eur. J. Biochem. 174*, 331. (b) Richardson, I. W., and Anthony, C. (1992) *Biochem. J. 287*, 709. (c) Harris, T. K., and Davidson, V. L. (1993) *Biochemistry 32*, 4362.
28. Itoh, S., Mure, M., Ogino, M., and Ohshiro, Y. (1991) *J. Org. Chem. 56*, 6857.
29. Yamada, K., Shimoda, M., and Okura, I. (1992) *J. Mol. Catal. 73*, 381.
30. Goodwin, M. G., and Anthony, C. (1996) *Biochem. J. 318*, 673.
31. Itoh, S., Fukui, Y., Ogino, M., Haranou, S., Komatsu, M., and Ohshiro, Y. (1992) *J. Org. Chem. 57*, 2788.
32. Carey, F. A., and Sundberg, R. J. (1990) *Advanced Organic Chemistry*, 3rd ed., Part A, Chapter 8, Plenum Press, New York and London.
33. Itoh, S., Kawakami, H., and Fukuzumi, S. (1997) *Chem. Commun*., 29.
34. *Handbook of Chemistry and Physics*, 61st ed. (1981) CRC Press, Boca Raton, FL.

BI9800092